RSC Advances

PAPER

View Article Online
View Journal | View Issue

Cite this: *RSC Adv.*, 2014, **4**, 35272

Distinct mechanical properties of nanoparticle-tethering polymers†

Tao Jiang, Liquan Wang and Jiaping Lin*

Mechanical properties of nanoparticle-tethering polymer systems were investigated by molecular dynamics simulations. The stress–strain behavior of nanoparticle-tethering polymers as a function of interaction strength and architecture parameters (polymer length and particle size) was examined. As the interaction strength between nanoparticles and polymers increases, the stress increases. The effects of architecture parameters on the stress are relatively complicated. With decreasing polymer length or increasing particle size, the stress increases at smaller strain, while at larger strain, the stress first increases and then decreases. The tensional moduli were also found to be dependent on the interaction strength and architecture parameters. The nanoparticle-tethering polymers exhibit enhanced mechanical properties relative to neat polymers and nanoparticle/polymer blends. It was found that the bond orientation, bond stretching, and nonbonding interaction play important roles in governing the mechanical properties of the nanoparticle-tethering polymer systems. The simulation results were finally compared with available experimental observations, and an agreement was obtained. The results gained through these simulations may provide useful guidance for designing high-performance hybrid materials.

Received 9th May 2014
Accepted 5th August 2014

DOI: 10.1039/c4ra04310c

www.rsc.org/advances

1. Introduction

Embedding inorganic nanoparticles into a polymer matrix can improve the mechanical, thermal, optical, and electronic properties of polymeric materials due to the nanoparticle–polymer interactions.[1–3] Covalently connecting the polymer chain to the nanoparticle could be a promising strategy for property improvement, because it can achieve good nanoparticle dispersions.[4,5] The nanoparticles which are linked to polymer chains can be sterically stabilized by surrounding polymers, and thus the nanoparticle agglomeration can be prevented.[6] The nanoparticle-tethering polymers and tethering polymer/polymer blends are specific organic/inorganic hybrids with better nanoparticle dispersions than nanoparticle/polymer blends. These special organic/inorganic molecules usually exhibit enhanced properties and may find potential applications in nanoreactors, energy storage, and medical care.[7–9]

Recently, many nanoparticles like C_{60} and polyoxometalate (POM) have been applied to chemically tether polymer chains through the modification of nanoparticle surfaces.[10–22] For example, Goel *et al.* synthesized silica (SiO_2)-tethering poly(*n*-butyl acrylate) brushes,[10] while Song and coworkers prepared fullerene-tethering poly(ethylene oxide).[13] So far most studies regarding the nanoparticle-tethering polymers are the nanoparticle dispersion in tethering polymer/polymer blends and the phase behavior of tethering polymers. For example, Lan *et al.* studied the dispersion of SiO_2 nanoparticles in SiO_2-tethering polystyrene (PS)/PS blends.[14] Uniform nanoparticle dispersions were observed when the molecular weight of matrix PS is roughly equal to or smaller than that of tethering PS. On the other hand, if the nanoparticles are strongly immiscible with the polymers, the nanoparticle-tethering polymers can phase-separate into ordered structures.[15–20] However, until now the related studies on the mechanical properties of nanoparticle-tethering polymers are limited.[23–28] Few primary investigations revealed that the hybrid systems possess unique mechanical properties. For example, the mechanical properties of triethoxysilane end-capped poly(tetramethylene oxide) (Si-PTMO)-modified CaO–SiO_2 hybrids were studied by Miyata *et al.*[23] It was found that the tensile strengths and Young's moduli are markedly influenced by the contents of CaO and PTMO. Al-Sagheer measured the dynamic mechanical properties of chemically bonded polyaramid–silica systems.[25] The storage moduli increase with increasing the silica content, and the moduli are retained at higher temperature. Due to the structural complexities of nanoparticle-tethering polymers and the limitations of experimental technology, many important issues, including the nanoparticle packing and acting

Shanghai Key Laboratory of Advanced Polymeric Materials, Key Laboratory for Ultrafine Materials of Ministry of Education, State Key Laboratory of Bioreactor Engineering, School of Materials Science and Engineering, East China University of Science and Technology, Shanghai 200237, China. E-mail: jlin@ecust.edu.cn; Tel: +86-21-64253370

† Electronic supplementary information (ESI) available: Details regarding the effects of interaction strength and architecture parameters on the stress–strain behavior of nanoparticle-tethering polymers and comparison among neat polymers, nanoparticle/polymer blends, and nanoparticle-tethering polymers. See DOI: 10.1039/c4ra04310c

mechanism of external factors on the mechanical properties, are little known.

Apart from the experiments, theory and simulation approaches, such as self-consistent field theory,[29] polymer reference interaction site model (PRISM) theory,[30] and molecular dynamics (MD),[31,32] have been applied to investigate the nanoparticle dispersions in nanoparticle-tethering polymer/polymer blends. Cao and coworkers studied the effects of grafting density, lengths of matrix polymer chains, and tethering chains on the nanoparticle dispersions in the polymer melts. It was found that increasing grafting density or tethering chain length leads to better dispersions, while increasing the matrix chain length leads to nanoparticle aggregations.[32] In terms of property evaluations, MD simulations are useful tools to get an insight into the mechanical properties of nanoparticle/polymer materials.[33–40] However, so far the MD studies of mechanical properties are mostly limited to nanoparticle/polymer blends, with focus on the effects of particle size,[33,34] particle–polymer interaction,[35] and particle shape.[36,37] Cho *et al.* investigated the effect of nanoparticle size on elastic properties of nanoparticle/polymer blends in bulk.[34] The Young's moduli were found to increase as the particle size decreases. Liu *et al.* studied the rubber reinforcements by employing idealized models of polymer networks and nanoparticles.[40] The dependencies of stress–strain behaviors on the nanoparticle amount, nanoparticle size, and nanoparticle–rubber interaction were examined, and the reinforcement mechanisms of rubber were preliminarily demonstrated. However, by now only limited studies of nanoparticle-tethering polymers are available. Many issues remain to be solved for this important category of materials. The success of the MD simulations makes it ready to be extended to examine the mechanical properties of nanoparticle-tethering polymers.

In the present work, we performed molecular dynamics simulations to investigate the mechanical properties of nanoparticle-tethering polymers. The effects of interaction strength and architecture parameters on the mechanical properties of nanoparticle-tethering polymers were examined. It was discovered that the mechanical properties can be enhanced by increasing nanoparticle–polymer interaction, particle size, or decreasing polymer length. However, too short polymer chains and too large nanoparticles both deteriorate the mechanical properties. A comparison of the mechanical properties among nanoparticle-tethering polymers, neat polymers, and nanoparticle/polymer blends was made. The simulation results were also compared with the available experimental observations. The bond orientations, effective bond lengths, and pairwise nonbonding potentials during the deformation process were examined to explain the relationship between the influencing factors and mechanical properties.

2. Method

We considered a system of nanoparticle-tethering polymers, and constructed a coarse-grained model, as typically shown in Fig. 1. The polymers were modeled as linear chains of L beads with diameter σ, where σ denotes the unit length. The nanoparticles were represented by Lennard-Jones (LJ) spheres of diameter d. We set the masses of the polymer beads and nanoparticles to m and $(d/\sigma)^3 m$ (m denotes the unit mass), so that a nanoparticle has the same density as a polymer bead.

In the molecular dynamics, simulating large polymeric systems or long polymeric processes requires so large computer resources that it cannot easily be carried out by traditional all-atom methods. To tackle the problem, "pseudo-atoms" are used to represent groups of atoms, instead of explicitly representing every atom of the system.[41] This reduced representation is called coarse-grained modeling. Coarse-grained molecular modeling allows the simulations to be run on larger length scales and longer time scales, providing realistic structural details. This method is widely applied to macromolecule systems and can well capture the feature of long polymer chains.[42,43]

In our coarse-grained MD model constructed, a polymer bead represents a segment consisting of number of monomers. The coarse-grained model was parameterized to match the experimental data. By mapping multiple real atoms into an interaction site, the model can correspond to a long polymer chain, and show the static and dynamic behavior characteristic of long chains. Such kind of modeling procedures is also widely adopted in the literatures.[44,45] Since each bead represents a segment consisting of number of monomers in the coarse-grained model, the hybrid systems we studied are in a rubbery or glassy state. In addition, the entanglement effects of polymer chains were not considered in this work.

To construct a hybrid molecule of polymer and nanoparticle, potentials that should be given are nonbonding potential U_{ij}, and bonding potential U_{bond}. The potential U_{ij}, describing the intermolecular interactions, is given by the modified LJ 12:6 potential acting between any pair of beads i and j:[46]

$$U_{ij} = \begin{cases} 4\varepsilon_{ij}\left[\left(\dfrac{\sigma}{r_{ij}-r_{\text{EV}}}\right)^{12} - \left(\dfrac{\sigma}{r_{ij}-r_{\text{EV}}}\right)^{6} - \left(\dfrac{\sigma}{r_{ij}^{c}}\right)^{12} + \left(\dfrac{\sigma}{r_{ij}^{c}}\right)^{6}\right], & r_{ij}-r_{\text{EV}} \le r_{ij}^{c} \\ 0, & r_{ij}-r_{\text{EV}} > r_{ij}^{c} \end{cases} \quad (1)$$

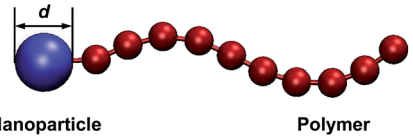

Fig. 1 Simulation model of nanoparticle-tethering polymer molecule.

where r_{ij}^{c} is the cutoff distance for $(r_{ij} - r_{EV})$, at which the potential is truncated and shifted to yield zero energy and force, and ε_{ij} is the interaction parameter between beads i and j. To account for the excluded volume effects of different interaction sites, we offset the interaction range by r_{EV}. r_{EV} are respectively chosen as $(d - \sigma)/2$, $d - \sigma$, and 0, for nanoparticle–polymer, nanoparticle–nanoparticle, and polymer–polymer interactions. The interactions are truncated at an attractive cutoff distance for the polymer–polymer and nanoparticle–polymer interactions ($r_{pp}^{c} = 2 \times 2^{1/6}$, $r_{np}^{c} = 2.5$) and a repulsive cutoff for the nanoparticle–nanoparticle interaction ($r_{nn}^{c} = 2^{1/6}$). The cutoff distance r_{ij}^{c} (interaction range) determines whether the interaction between beads i and j is attractive or repulsive. When the value of r_{ij}^{c} is larger than $2^{1/6}$, the interaction is attractive, otherwise, repulsive.[47] Therefore, in the present work, the polymer–polymer and nanoparticle–polymer interactions are attractive, while the nanoparticle–nanoparticle interaction is repulsive. The attraction between polymers can ensure a positive thermal expansion coefficient, while the repulsion between nanoparticles can reduce the nanoparticle agglomeration.[48]

In the simulations, all quantities adopted reduced units. The interaction parameter ε_{ij} (interaction strength) has the energy unit of γ. The reduced unit can be converted into the real unit. The detailed information can be found in our previous work.[47] Since it is not our aim to study a specific polymer or nanoparticle, the interaction parameters ε_{pp} (between polymer beads) and ε_{nn} (between nanoparticles) were fixed as unity for convenience. However, the interaction parameter ε_{np} (between nanoparticles and polymers) was chosen to be variable, simulating a different attractive interfacial interaction.

The bonding potential U_{bond}, is given by the modified finite extensible nonlinear elastic (FENE) potential:[40]

$$U_{FENE} = -0.5kR_0^2 \ln\left[1 - \left(\frac{r - R_{EV}}{R_0}\right)^2\right] \quad (2)$$

where $k = 30\varepsilon_{pp}/\sigma^2$, $R_0 = 1.5\sigma$, and R_{EV} is zero for bonds between polymer beads but equal to $(d - \sigma)/2$ for bonds between polymer bead and nanoparticle. We did not adopt a harmonic potential, because the harmonic bonds can extend infinitely upon the tension, exhibiting unphysical stretching. In contrast, the FENE bonds can only extend to finite length, which can generate mechanical properties with small deviation from molecules with rigid bonds.[49] In addition, the spring constant k of 30 is strong enough to restrict the maximum extension of bonds and thereby avoid chain crossing.[50,51] On the other hand, it is also small enough so that we can use a larger time step Δt comparable with the one for a fluid of Lennard-Jones particles.[50]

In our MD simulations, to generate the initial configurations, we constructed a large system of low volume fraction, which was compressed to the volume fraction of 0.45. The initial box lengths were respectively chosen as 20.7 and 22.7 for neat polymers containing 315 chains ($L = 24$), and nanoparticle-tethering polymers with 315 molecules ($L = 24$, $d = 2\sigma$). For various polymer lengths or nanoparticle diameters, initial box length and volume fraction were fixed. As a result, the chain number was changed correspondingly. For the blends, the initial volume fraction was also set as 0.45. Based on the initial configurations, the NPT ensemble with $T = 1.0$ and $P = 0$ was adopted by using the Nose–Hoover thermostat and barostat, similar to that published in the literatures.[52] The selection of the pressure yields an equilibrium density of polymer beads larger than 0.7 corresponding to its bulk state, according to Smith's work.[53] Under the NPT ensemble, the volume fraction is variable, but at equilibration the volume fraction is roughly equivalent for each system. Note that initial existing overlaps between polymer beads and nanoparticles were removed by carrying out a standard MD simulation with a soft repulsive potential:[50]

$$U_{soft} = \begin{cases} A\left[1 + \cos\left(\frac{\pi r}{\sqrt[6]{2}\sigma}\right)\right], & r \le \sigma \\ 0, & r > \sigma \end{cases} \quad (3)$$

where the coefficient $A = 20.0$. During the simulations, periodic boundary conditions were imposed, and the velocity-Verlet algorithm[54,55] was used to integrate the equations of motion with a time step $\Delta t = 0.004\tau$ (τ denotes the unit time). We carried out 5×10^7 MD steps for all the structures so that the computing time was long enough for the system to achieve an equilibrium state. The gyration radius of the system arrived at a plateau and fluctuated at a low level, suggesting that the system reached an equilibrium condition. The structures and dynamics data of the last 5×10^5 steps were collected for ensemble average.

Regarding the calculations of mechanical properties, tension tests were performed after enough equilibration by a uniaxial deformation on the simulation box along the z direction under the NVT ensemble with $T = 1.0$ and $\Delta t = 0.001\tau$. As the box is elongated in the z direction, the box lengths in the x and y directions are changed simultaneously to keep the system volume constant. To make more physical sense, materials are assumed to have no volume change and incompressible, and the Poisson's ratio μ is 0.5.[56] The uniaxial deformation occurs over a time period of 100τ. The strain rate was set as $0.0327/\tau$. The strain rate is the same as the simulations from Gao *et al.*,[57] where the strain rate is comparable with the segmental relaxation. The tension stress σ in the z direction was calculated by the deviatoric part of the stress tensor[58,59]

$$\sigma = (1 + \mu)(-P_{zz} + P) = 3(-P_{zz} + P)/2 \quad (4)$$

where $P = \sum_{\alpha} P_{\alpha\alpha}/3$ is the hydrostatic pressure. The diagonal component $P_{\alpha\alpha}$ of pressure tensor is the negative value of the average virial stress $\sigma_{\alpha\alpha}$ in the α direction, and $\sigma_{\alpha\alpha}$ is given by[33]

$$\sigma_{\alpha\alpha} = -\frac{1}{V}\sum_{i}\left(m^i v_\alpha^i v_\alpha^i + \frac{1}{2}\sum_{j\neq i}^{j} F_\alpha^{ij} r_\alpha^{ij}\right) \quad (5)$$

where V is the volume of simulation box, m^i is the mass of atom i, v_α^i is the α-component of the velocity of atom i, F_α^{ij} is the α-component of the force between atoms i and j, and r_α^{ij} is the α-component of the distance between atoms i and j. Note that for stress average, several tension tests were performed based

on above collected equilibrated structures. All MD runs were carried out by using the large scale atomic/molecular massively parallel simulator (LAMMPS), which was developed by Sandia National Laboratories.[60]

In this work, we generated bond order diagrams (BOD)[61,62] to characterize the packing structures of nanoparticles. The stereographic projections of the nearest-neighbor bonds between nanoparticles were constructed as follows. First, all nearest-neighbor vectors about central particles were determined and normalized to unit length. Then, the vectors were placed at a common origin so that their endpoints are located on the unit sphere. Finally, the distribution of the points on the sphere was represented by stereographic projections along three coordinate axes. The diagrams obtained can reveal the global symmetry of the sample. Systems with highly correlated neighbor directions (*e.g.*, bulk crystalline materials) show distinct groupings of points on the sphere surface, in contrast, a disordered system appears as points randomly distributed on the surface.

For further characterizing the packing structures of nanoparticles, pair correlation function $g(r)$ between the nanoparticles was also calculated. The $g(r)$, defined as the probability of finding the particles separated by distance r, is expressed by $\langle n(r)\rangle/4\pi r^2\rho_0\Delta r$,[63] where Δr is a given thickness of spherical shell, $\langle n(r)\rangle$ is the average particle number within the shell between r and $r + \Delta r$, and ρ_0 is the entire number density of particles. It gives a measure of spatial organization of particles about the central particles, and can be used to demonstrate the dispersion and packing state of nanoparticles.[40]

3. Results and discussion

In this work, we mainly focused on the mechanical properties of nanoparticle-tethering polymers. The strength of nonbonding interaction and architecture parameters such as polymer length and particle size are important parameters governing the structures and mechanical properties of nanoparticle/polymer hybrid systems. Influences of these factors were examined.

3.1. Mechanical properties of nanoparticle-tethering polymers

In this subsection, the stress–strain behaviors of nanoparticle-tethering polymers at various strengths of nonbonding interactions between nanoparticles and polymers ε_{np} were firstly investigated. The ε_{np} was changed from 1.0 to 12.0. The stress–strain data were captured by uniaxial tensions at a constant strain rate and $T = 1.0$. The polymer bead number and nanoparticle diameter were chosen as $L = 24$ and $d = 2\sigma$, respectively. The mass of nanoparticle was set to be $8m$ so as to keep its density identical with polymer beads.

Representative stress–strain curves of nanoparticle-tethering polymers at various ε_{np} are shown in Fig. 2a. It can be seen that as ε_{np} increases, the stress at the same strain increases rapidly, which becomes more prominent at larger strain. In addition, obvious and well-defined yield points emerge in the stress–strain curves at larger ε_{np} (*e.g.*, $\varepsilon_{np} = 12.0$). At smaller ε_{np}, there

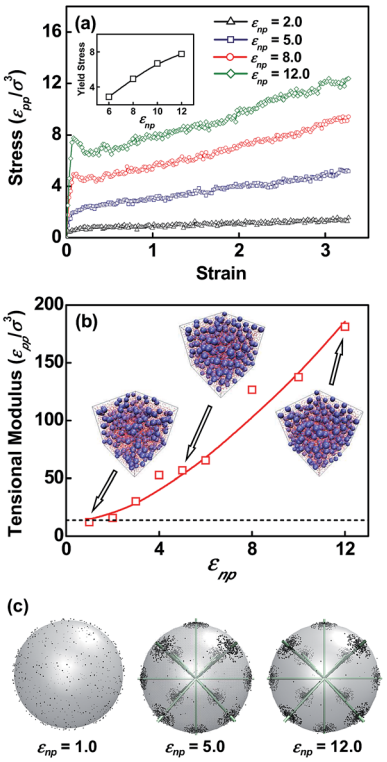

Fig. 2 (a) Stress–strain curves at various ε_{np} for the nanoparticle-tethering polymers with $L = 24$, and $d = 2\sigma$. The insert shows the yield stress as a function of ε_{np}. (b) Tensional moduli of the nanoparticle-tethering polymers as a function of ε_{np}. The dashed line denotes the tensional moduli of neat polymers. The insert shows the typical morphology snapshots at $\varepsilon_{np} = 1.0$, 5.0, and 12.0. The polymer beads are denoted with red points to avoid obscuring the nanoparticles. (c) BOD of nanoparticles for nearest neighbors at various ε_{np}. The lines at $\varepsilon_{np} = 5.0$ and 12.0 indicate the BOD of an ideal FCC structure.

are no obvious yield points. A plot of yield stress (stress at the yield point) with respect to ε_{np} is presented in the insert. As can be seen, the yield stress increases with increasing ε_{np}. Fig. 2b shows the tensional moduli of the nanoparticle-tethering polymers as a function of ε_{np}. The tensional modulus (E) was determined by the slope of stress–strain curve within 2% strain.[34] E was found to increase with increasing ε_{np}. The tensional moduli at $\varepsilon_{np} = 1.0$ are lower than those of neat polymers (denoted by the dashed line), without exhibiting a reinforcement effect. It suggests that the polymer reinforcement by attaching nanoparticles can be only achieved at stronger nanoparticle–polymer nonbonding interaction. The insert shows the typical morphology snapshots at $\varepsilon_{np} = 1.0$, 5.0, and 12.0. The nanoparticle packing is ordered for $\varepsilon_{np} = 5.0$ and 12.0. The bond order diagrams (BOD) were applied to describe the packing feature of nanoparticles. The packing geometry can be determined according to the distribution of projected points on the sphere surface.[61] Fig. 2c shows the BOD of nanoparticles for nearest neighbors at various ε_{np}. At $\varepsilon_{np} = 1.0$, the projected points are distributed randomly on the sphere surface, suggesting the nanoparticle packing is not ordered. At $\varepsilon_{np} = 5.0$ and 12.0, there are eight point groups along the space diagonals and

four point groups along the four-fold directions. The pattern agrees with the BOD of an ideal face-centered-cubic (FCC) structure, as shown by lines in Fig. 2c. It indicates that the nanoparticles are packed approximately in a FCC manner. The FCC packing of nanoparticles at $\varepsilon_{np} = 5.0$ and 12.0 can be further verified by the position ratio $1 : \sqrt{2} : \sqrt{3} : 2$ of typical peaks in $g(r)$ (see Fig. S1 in ESI†).

In Fig. 2a, yield point appears in the stress–strain curve of nanoparticle-tethering polymers at larger ε_{np}, which is the general feature of glassy or crystalline polymers. To explain this phenomenon, we calculated the glass transition temperature T_g of the nanoparticle-tethering polymers for various ε_{np}. The T_g value can be estimated by the temperature at break point in the effective volume per monomer.[64] Due to the indetermination of monomer number in hybrid systems, we used the total volume $V(T)$ instead, which were obtained through annealing a high-temperature system and then equilibrating the system. The V as a function of T at various ε_{np} were plotted in Fig. 3. For each ε_{np}, V increases linearly with increasing T below or above a certain temperature. By linear fitting, the intersection of two fitted lines was obtained, where the temperature is T_g.[44,64] T_g were estimated to be 0.66, 0.87, and 1.33, for $\varepsilon_{np} = 5.0$, 8.0, and 12.0. It indicates that as ε_{np} increases, the T_g increases.

For $\varepsilon_{np} = 12.0$, the T_g becomes higher than the temperature applied ($T = 1.0$), therefore the nanoparticle-tethering polymers exhibit a glassy state at $T = 1.0$. The nanoparticles were observed to have an ordered packing manner below T_g, although the nanoparticles are frozen (manifested by the diffusion coefficient of nanoparticles, see Fig. S2 in ESI†). With decreasing ε_{np} to 8.0, although the T_g is lower than 1.0, the emergence of yield point could be due to the ordered packing of nanoparticles. The ordered nanoparticle packing makes the nanoparticle-tethering polymers behave like crystalline polymers. Further decreasing ε_{np}, the T_g is much lower than 1.0, and the temperature may have a more pronounced effect on the stress–strain behavior than the nanoparticle ordering. Usually, at a temperature above T_g, no yield point appears in a stress–strain curve.[65] Therefore, the dominated action of the temperature could lead to no yield point in the stress–strain curve. From above results, it can be concluded the examined temperature and nanoparticle ordering were critical in controlling the shape of stress–strain curves.

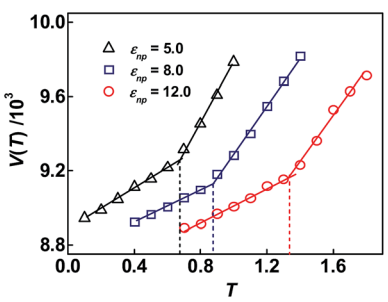

Fig. 3 Plot of the total volume $V(T)$ as a function of the temperature T at various ε_{np}.

In order to get deep insight into the influencing mechanisms of ε_{np} on the stress–strain behavior, the bond orientation, effective bond length, and nonbonding potential were examined. The results are presented in Fig. 4a–c. The bond orientation was characterized by the second-order Legendre polynomials $\langle P_2 \rangle$. The $\langle P_2 \rangle$ is given by $(3\langle \cos^2\theta \rangle - 1)/2$,[40] where θ is the angle between bonds and the deformed direction. The definition of θ can be viewed from the inset of Fig. 4a. This parameter reflects the chain alignment. $\langle P_2 \rangle = 1.0$ and -0.5 correspond to perfect alignments parallel and perpendicular to the deformed direction, respectively. As shown in Fig. 4a, the $\langle P_2 \rangle$ becomes larger with increasing ε_{np} at any equal strain for smaller ε_{np}. However, the $\langle P_2 \rangle$ is almost unaffected by the ε_{np} as its value is larger. The effective bond length $l_{b,eff}$ is the average of $(l_b - R_{EV})$ for all bonds, characterizing the bond stretching degree. Fig. 4b shows that the $l_{b,eff}$ increases gradually with increasing the strain, although it has only a slight increase at $\varepsilon_{np} = 2.0$. It implies that the bonds become more stretching during the tension process. Moreover, as ε_{np} increases the $l_{b,eff}$ increases more remarkably with the strain, suggesting that the increase in bond stretching degree is more marked for larger

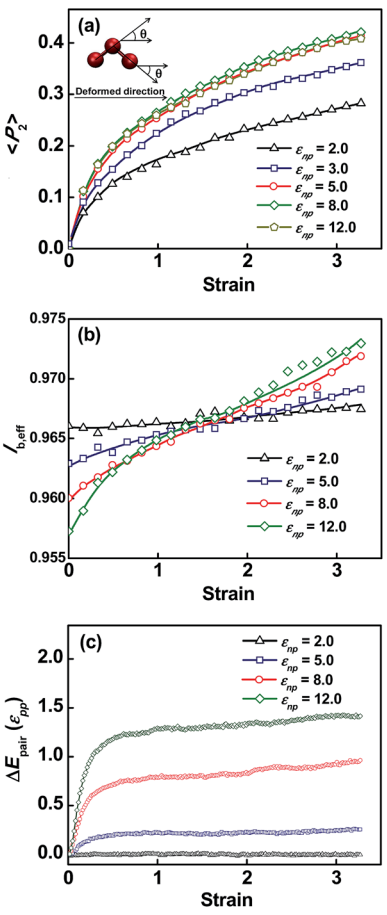

Fig. 4 (a) Bond orientations $\langle P_2 \rangle$ with respect to the strain at various ε_{np}. The insert shows the sketch of the definition of angle θ. (b) Effective bond lengths $l_{b,eff}$ *versus* the strain at various ε_{np}. (c) Changes of nonbonding potential ΔE_{pair} between deformed and undeformed states with respect to the strain at various ε_{np}.

ε_{np}. At smaller strain, the $l_{b,eff}$ for larger ε_{np} is smaller than that for smaller ε_{np}, due to the stronger attraction between nanoparticles and polymers. However, at larger strain, the $l_{b,eff}$ is larger for larger ε_{np}, because the average bond length mainly comes from the bonds between polymers.[40]

The bond orientation and stretching contribute to the stress in terms of conformational entropy. The contributions from interaction enthalpy can be manifested by the change of nonbonding potential ΔE_{pair}. ΔE_{pair} is the difference of total nonbonding potentials between deformed and undeformed states. The ΔE_{pair} as a function of the strain at various ε_{np} are shown in Fig. 4c. The nonbonding potentials increase rapidly to plateaus, and then have slight changes at larger strain, indicating that nonbonding interactions contribute to the increase in stress only at smaller strain. From Fig. 4c, we can also see that the ΔE_{pair} possesses a larger value at larger ε_{np}. It means that nonbonding interactions make greater contributions to the stress.

Usually the generated tensional stress arises from the loss of conformational entropy and the increase in interaction enthalpy.[66,67] We learn that the nanoparticle-tethering polymers have a higher bond orientation for larger ε_{np}, and the increase in bond stretching degree is more obvious (Fig. 4a and b). They both result in the larger entropy loss as ε_{np} is larger. On the other hand, the nonbonding potential has a larger increase upon deformation for larger ε_{np} (Fig. 4c), therefore, the enthalpy gain is also larger for larger ε_{np}. Under the cooperative action of entropy and enthalpy, the nanoparticle-tethering polymers exhibit higher stress and modulus at larger ε_{np} as shown in Fig. 2a and b. We can also learn from Fig. 4 that the entropy tends to dominate the increase in stress with the strain at larger strain, since the nonbonding potential has no obvious change at larger strain.

In addition to the interaction strength, we studied the effects of architecture parameters (*i.e.*, polymer length and particle size) on the stress–strain behaviors of nanoparticle-tethering polymers. The polymer length is denoted by the bead number L in one polymer chain. The stress–strain curves for the nanoparticle-tethering polymers with various L at $\varepsilon_{np} = 5.0$ are shown in Fig. 5a. The nanoparticle diameter was fixed as 2σ. For larger L, the stress increases rapidly with increasing the strain, while for smaller L, the stress has a slight increase or reaches a plateau following a yield point. The insert shows the relations between stress and L at smaller ($\varepsilon = 0.049$) and larger ($\varepsilon = 3.27$) strains. At smaller strain, the stress decreases with increasing L, while at larger strain, the stress first increases and then decreases. Fig. 5b presents the tensional moduli of nanoparticle-tethering polymers with various L. It can be seen that the tensional moduli E decrease as L increases from 4 to 36. In the insert, the structures for $L = 4$ and 36 shows ordered packing of nanoparticles. A hexagonally closed packing of nanoparticles for $L = 4$ and a FCC packing for $L = 36$ were observed from the BOD and plot of $g(r)$ (Fig. S3 in ESI†).

In Fig. 5a, for polymers with short chains, the stress–strain curves exhibit features of glassy or crystalline polymers. We calculated the T_g for the nanoparticle-tethering polymers with various L to explain this phenomenon. Fig. 5c shows the total

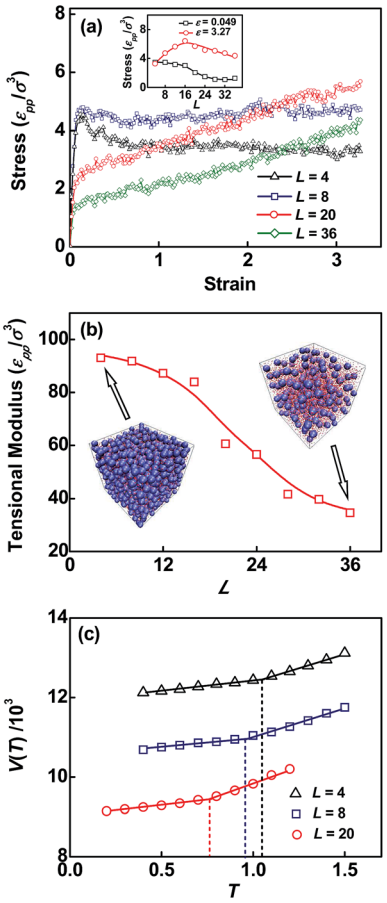

Fig. 5 (a) Stress–strain curves for the nanoparticle-tethering polymers with various L at $\varepsilon_{np} = 5.0$. The nanoparticle diameter is 2σ. The insert shows the relations between stress and L at smaller ($\varepsilon = 0.049$) and larger ($\varepsilon = 3.27$) strains. (b) Tensional moduli of the nanoparticle-tethering polymers as a function of L. The insert shows the typical morphology snapshots for $L = 4$, and $L = 36$. (c) Total volumes $V(T)$ as a function of T for various L.

volumes $V(T)$ as a function of T for various L. According to the intersections of fitted lines, the T_g were obtained to be 1.05, 0.95 and 0.77, for $L = 4$, 8, and 20. The T_g decreases with increasing L. For $L > 20$, the T_g is much lower than 1.0, and the temperature dominates the shape of the stress–strain curve (without yield point). For $L = 8$, although the T_g is lower than 1.0, the nanoparticle ordering makes the system behave like crystalline polymers (with a yield point in the stress–strain curve). For $L = 4$, $T = 1.0$ is lower than the glass transition temperature. The cooperative action of temperature and nanoparticle ordering leads to the emergence of the yield point and the strain softening regime in stress–strain curve (Fig. 5a).

The dependence of stress–strain behavior on L can be explained by the bond orientation, effective bond length, and nonbonding potential. The $\langle P_2 \rangle$ and $l_{b,eff}$ as functions of the strain for various L are shown in Fig. 6a and b. Fig. 6a shows that the $\langle P_2 \rangle$ increases with increasing the strain for any L. The $\langle P_2 \rangle$ is slightly affected by L at smaller strain, while at larger strain it differs significantly for various L. The insert shows the $\langle P_2 \rangle$ with respect to L at larger strain ($\varepsilon = 3.27$). It first increases and then

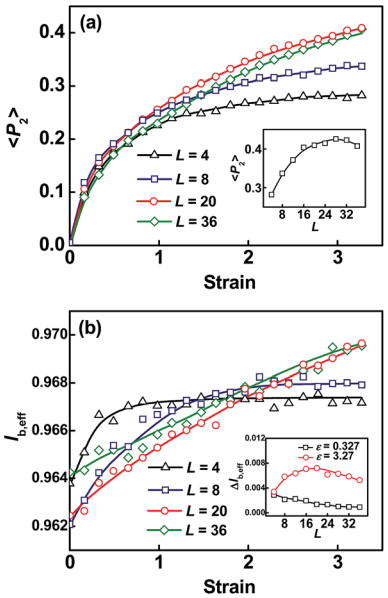

Fig. 6 (a) Bond orientations $\langle P_2 \rangle$ *versus* the strain for various L. The insert shows the $\langle P_2 \rangle$ with respect to L at larger strain ($\varepsilon = 3.27$). (b) Effective bond lengths $l_{b,eff}$ *versus* the strain for various L. The insert shows the increased amount in $l_{b,eff}$ relative to the undeformed state as a function of L at smaller ($\varepsilon = 0.327$) and larger ($\varepsilon = 3.27$) strains.

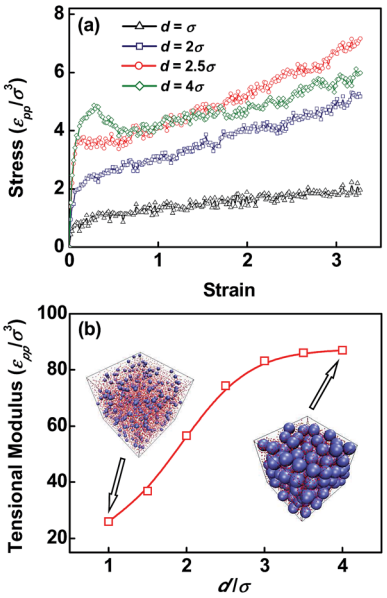

Fig. 7 (a) Stress–strain curves for the nanoparticle-tethering polymers with various d at $\varepsilon_{np} = 5.0$ and $L = 24$. (b) Tensional moduli of the nanoparticle-tethering polymers as a function of d. The insert shows the typical morphology snapshots for $d = \sigma$, and $d = 4\sigma$.

has a slight decrease as L increases. Fig. 6b indicates that the $l_{b,eff}$ increases gradually with the strain for larger L, but it increases rapidly to a plateau for smaller L. The insert shows the increased amount in $l_{b,eff}$ relative to the undeformed state as a function of L at smaller ($\varepsilon = 0.327$) and larger ($\varepsilon = 3.27$) strains. At smaller strain, the $\Delta l_{b,eff}$ decreases with increasing L, while at larger strain, the $\Delta l_{b,eff}$ exhibits a maximum value for $L = 20$. It means that $l_{b,eff}$ increases with the strain more markedly for smaller L at smaller strain, leading to larger entropy loss for smaller L. Besides the entropy loss, the nanoparticle-tethering polymers with smaller L have larger enthalpy gain at smaller strain (larger ΔE_{pair}, see Fig. S4†). The entropy and enthalpy cooperatively contribute to the higher stress and modulus for smaller L as shown in Fig. 5a and b. At larger strain, the enthalpy gain (ΔE_{pair}) is still larger for smaller L, but the entropy loss first increases and then decreases with increasing L. It is shown that at larger strain, the stress first increases and then decreases with increasing L (Fig. 5a). Therefore, the stress is dominated by the entropy for smaller L, while it is controlled by the cooperative action of entropy and enthalpy for larger L.

We also studied the stress–strain curves for nanoparticle-tethering polymers with various particle sizes d at $\varepsilon_{np} = 5.0$ and $L = 24$, as shown in Fig. 7a. By changing the particle size d from σ to 2σ, and then to 2.5σ, the stress increases continuously. Further increasing d up to 4σ, the stress at the same strain still increases at smaller strain ($\varepsilon < 0.6$), while the stress decreases as the strain is larger than 1.7. The results indicate that too large nanoparticles would deteriorate the mechanical properties at larger strain. The tensional moduli E as a function of d are shown in Fig. 7b. E increases gradually as d increases, but the increased slope decreases. From the insert, it can be seen that the nanoparticles become crowded with increasing d to 4σ, and the packing of nanoparticles becomes disordered. This is manifested by the features of BOD and $g(r)$ (see Fig. S5a†).

To analyze the effect of particle size on the stress–strain behavior, the bond orientations, effective bond lengths, and nonbonding potentials were calculated for various d, as shown in Fig. 8. From Fig. 8a, it can be seen that the $\langle P_2 \rangle$ increases with the strain for any d. As d increases, the $\langle P_2 \rangle$ first becomes larger and then smaller. This can be viewed from a plot of $\langle P_2 \rangle$ *versus* d at larger strain ($\varepsilon = 3.27$, see the insert). The $l_{b,eff}$ as a function of the strain for various d are shown in Fig. 8b. $l_{b,eff}$ increases gradually with the strain for any d, and the increase in $l_{b,eff}$ becomes more marked as d increases. The above results reveal that when d is smaller, the entropy loss increases with increasing d. In addition to entropy loss, the enthalpy gain increases with increasing d for any d (ΔE_{pair} increases, see Fig. 8c). Therefore, the cooperative increases in entropy loss and enthalpy gain contribute to the increases in stress and modulus with d for smaller d (Fig. 7a and b). As the value of d is larger, the actions of entropy and enthalpy on the stress are similar at smaller strain. At larger strain, the enthalpy gain still increases as d increases (see Fig. 8c). According to the result as shown in Fig. 7a, for larger d the stress decreases with increasing d at larger strain. Therefore, the entropy loss has to decrease with d, which can be rationalized by the decrease of bond orientation with d (Fig. 8a). It can be found that the entropy tends to dominate the stress at larger strain for larger d.

In this work, we studied the mechanical properties of nanoparticle-tethering polymers with FENE bonds. As mentioned above, the spring constant of FENE bonds can restrict the stretching of bonds,[50] thereby influence the mechanical

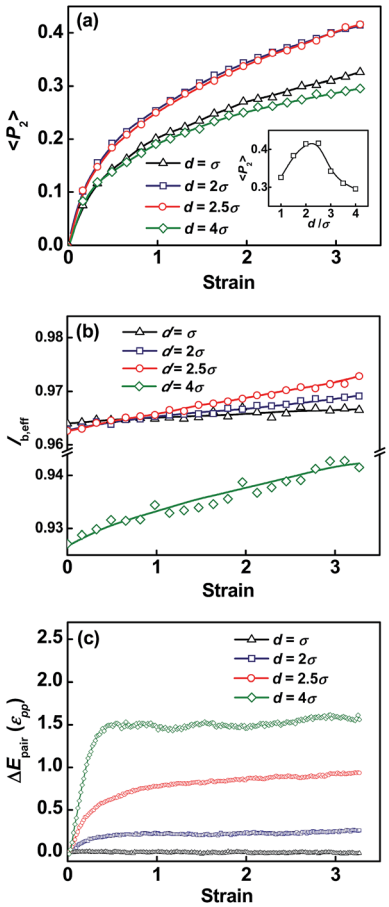

Fig. 8 (a) Bond orientations $\langle P_2 \rangle$ *versus* the strain for various d. The insert shows the $\langle P_2 \rangle$ with respect to d at larger strain ($\varepsilon = 3.27$). (b) Effective bond lengths $l_{b,eff}$ *versus* the strain for various d. (c) ΔE_{pair} *versus* the strain for various d.

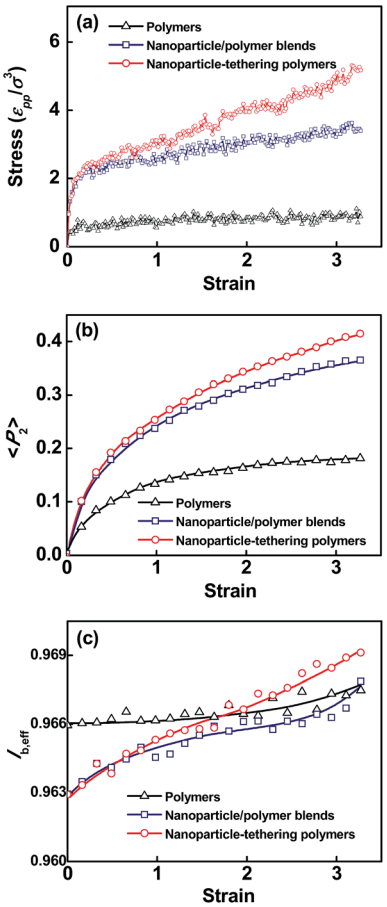

Fig. 9 (a) Stress–strain curves for the neat polymers, nanoparticle/polymer blends, and nanoparticle-tethering polymers at $T = 1.0$. The polymer length $L = 24$, the nanoparticle diameter $d = 2\sigma$, and the nanoparticle–polymer interaction strength $\varepsilon_{np} = 5.0$. (b) Bond orientations $\langle P_2 \rangle$ with respect to the strain for the three systems. (c) Effective bond lengths $l_{b,eff}$ as a function of the strain for the three systems.

properties in terms of conformational entropy. The FENE bonds play an important role in controlling the mechanical properties, which produce small deviation in mechanical properties from rigid bonds,[49] exhibiting more physical behavior. However, in this work, the contribution of bonding interaction to the mechanical properties was observed to be relatively smaller than the nonbonding interaction, ascribed to small increase in chain stretching degree upon the tension.

3.2. Comparison with neat polymers and nanoparticle/polymer blends

In this subsection, we made a comparison of the mechanical properties among nanoparticle-tethering polymers, neat polymers, and nanoparticle/polymer blends. The numbers of polymer chains in these systems were equivalent, and in nanoparticle-containing systems the nanoparticle numbers were kept constant. The polymer length was set to be 24 and the nanoparticle diameter was set to be 2σ. The mass of nanoparticle was set as $8m$ and the nanoparticle–polymer interaction strength was $\varepsilon_{np} = 5.0$. The stress–strain behaviors of these systems were simulated at $T = 1.0$, which is higher than their glass transition temperatures (see Fig. S6a†).

Fig. 9a shows the stress–strain curves for the three systems. As can be seen, the neat polymers possess low stress at any strain. By introducing nanoparticles through physical blending or chemical coupling, the stress can be enhanced significantly. At smaller strain ($\varepsilon < 0.5$), the stress of nanoparticle-tethering polymers is almost the same as that of nanoparticle/polymer blends at the same strain. However, when the strain is larger than 0.5, the stress of nanoparticle-tethering polymers is higher than that of nanoparticle/polymer blends. Such a phenomenon becomes more prominent at larger strain. The tensional moduli E were $13.4\varepsilon_{pp}/\sigma^3$, $53.3\varepsilon_{pp}/\sigma^3$, and $56.6\varepsilon_{pp}/\sigma^3$ for the neat polymers, nanoparticle/polymer blends, and nanoparticle-tethering polymers, respectively. It can be found that the nanoparticle/polymer blends and nanoparticle-tethering polymers have higher tensional moduli than the neat polymers, and the moduli of nanoparticle-tethering polymers exhibit a slight increase relative to the nanoparticle/polymer blends.

The nanoparticle-tethering polymers exhibit the enhanced mechanical properties relative to neat polymers or nanoparticle/polymer blends at strong nanoparticle–polymer attraction. Fig. 9b and c shows the bond orientations and

effective bond lengths as functions of the strain for three systems. The $\langle P_2 \rangle$ was found to increase with increasing the strain. Compared with neat polymers, higher bond orientations were observed in the nanoparticle/polymer blends and nanoparticle-tethering polymers. And the bond orientation of nanoparticle-tethering polymers is a little higher than that of nanoparticle/polymer blends. Fig. 9c shows that the increase in $l_{b,eff}$ with the strain is the most marked for nanoparticle-tethering polymers, while the least marked for neat polymers. It can be found that the nanoparticle-tethering polymers have higher bond orientation and more marked increase in bond stretching degree compared to neat polymers and nanoparticle/polymer blends. These make the nanoparticle-tethering polymers possess larger entropy loss under the tension. In addition, the nanoparticle-tethering polymers exhibit larger increase in E_{pair} than neat polymers and nanoparticle/polymer blends, leading to larger enthalpy gain (see Fig. S6b†). The larger entropy loss and enthalpy gain both contribute to the result that the nanoparticle-tethering polymers deform stronger.

3.3. Comparison with available experimental observations

Some experimental observations regarding the nanoparticle reinforcement are available in the literature for supporting our predictions. Mahfuz *et al.* studied the mechanical properties of nylon-6 loaded with SiO_2 nanoparticles.[28] Nylon is a semi-crystalline thermoplastic polymer, whose melting point and glass transition temperature are higher than the room temperature. In SiO_2/nylon system, SiO_2 nanoparticles have a strong affinity with nylon chains due to their large surface area-to-volume ratio, and there are strong hydrogen bonds between the amide groups of nylon and the surface bound OH groups of SiO_2 particles. The hydrogen-bonding interaction can reduce the interaction between nanoparticles, thereby reducing the nanoparticle agglomeration and improving the dispersion. By incorporating pristine SiO_2 particles into nylon, the improvements over neat nylon in tensile strength and Young's modulus were 36% and 28%. When the SiO_2 particles were functionalized by using a silane coupling agent, a covalent Si–O–Si bond between nylon and SiO_2 particle was formed. The incorporation of functionalized SiO_2 particles resulted in 76% and 55% improvements in strength and modulus.

In the present work, we used MD calculations to reproduce the experimental results. To simulate the reinforcement effect of SiO_2 nanoparticles on the nylon, we examined the stress–strain behaviors in the glassy states for the neat polymers, nanoparticle/polymer blends, and tethering polymer/polymer blends (*i.e.*, functionalized nanoparticle/polymer blends). We set following simulation conditions corresponding to the experiments. In the nanoparticle/polymer blends, 189 nanoparticles were incorporated into 315 polymer chains, and in the tethering polymer/polymer blends, the number and volume fraction of nanoparticles were the same. The glassy states were prepared by a quench from temperature $T = 1.0$ to a glassy temperature $T = 0.2$ at constant pressure $P = 0$. Tension tests along the z direction were carried out under the NPT ensemble with $P_{xx} = P_{yy} = 0$ after enough equilibration. For each system, five tension tests were performed to obtain the average value of stress based on the equilibrated structures which were collected in the last 5×10^5 steps. The parameters were set as follows: $L = 24$, $d = 2\sigma$, and $\varepsilon_{np} = 5.0$. A coarse-grained chain with 24 beads represents the long nylon chain. The nonbonding nanoparticle–polymer interaction is strongly attractive based on the molecular nature of nylon and SiO_2, while the interaction between nanoparticles is purely repulsive to reduce the nanoparticle agglomeration.

Fig. 10a shows the average stress–strain curves simulated for the three systems. The initial elastic regime, subsequent strain softening regime, and last strain hardening regime can be clearly seen for the three curves. The insert indicates the nearly linear stress–strain behaviors at strain $\varepsilon < 0.05$. By a linear fitting within 2% strain, tensional moduli E were obtained to be $37.0\varepsilon_{pp}/\sigma^3$, $56.0\varepsilon_{pp}/\sigma^3$, and $61.3\varepsilon_{pp}/\sigma^3$ for the neat polymers, nanoparticle/polymer blends, and tethering polymer/polymer

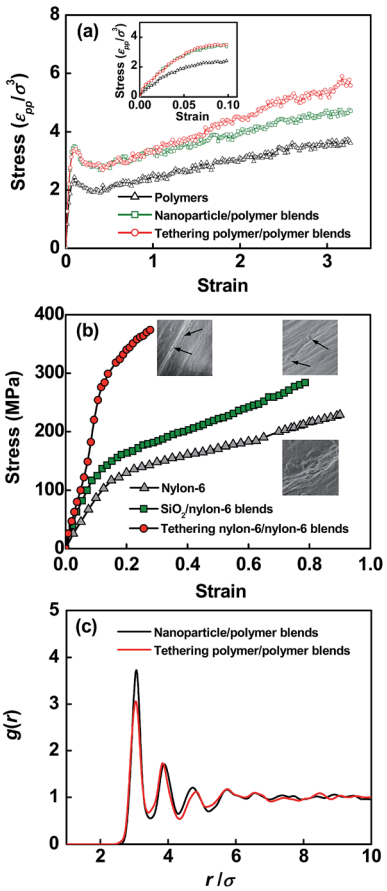

Fig. 10 (a) Stress–strain curves for the neat polymers, nanoparticle/polymer blends, and tethering polymer/polymer blends in the glassy state ($T = 0.2$). The insert indicates the stress–strain behaviors at small deformations. (b) Stress–strain curves for the neat nylon, SiO_2/nylon blends, and SiO_2-tethering nylon/nylon blends of Mahfuz's experiments. The insert shows the local structures of the three materials (reproduced from ref. 28 with permission of IOP Publishing). (c) Pair correlation functions $g(r)$ between the nanoparticles for the nanoparticle/polymer blends, and tethering polymer/polymer blends at $T = 0.2$.

blends. That is to say the improvements in tensional modulus over neat polymers are respectively 51% and 66% for nanoparticle/polymer blends, and tethering polymer/polymer blends. For a clear comparison, the stress–strain curves for neat nylon, SiO_2/nylon blends, and SiO_2-tethering nylon/nylon blends of Mahfuz's experiments were replotted in Fig. 10b. The tethering nylon/nylon blends were found to possess higher stress relative to neat nylon and SiO_2/nylon blends. Our simulation results demonstrate the enhanced mechanical properties of tethering polymer/polymer blends in glassy state, which are in qualitative accordance with Mahfuz's experimental observations. In addition, the local SEM morphologies of filament cross-section for the three materials of their experiments are shown in the insert of Fig. 10b. From the SEM images, they found that the nanoparticle clusters (outlined by arrows) emerge in SiO_2/nylon blends. However, in SiO_2-tethering nylon/nylon blends, the nanoparticles disperse in the form of individual nanoparticle (outlined by arrows). The better nanoparticle dispersion in tethering nylon/nylon blends was then proved by the simulations. The $g(r)$ between the nanoparticles for the nanoparticle/polymer blends, and tethering polymer/polymer blends at $T = 0.2$ are shown in Fig. 10c. Compared to the nanoparticle/polymer blends, the peak intensity of tethering polymer/polymer blends at $r = 3\sigma$ is smaller, suggesting that the nanoparticles are less close to each other.[31] In other words, the tethering polymer/polymer blends have better nanoparticle dispersion than nanoparticle/polymer blends.

Comparing Fig. 10a with Fig. 9a, we also learn that the reinforcing efficiency of rubbery polymers by introducing spherical nanoparticles is much higher than that of glassy polymers. The tensional modulus can be improved by 322% through attaching nanoparticles for rubbery polymers (Fig. 9a), while for glassy polymers the improvement in tensional modulus is 66% (Fig. 10a). That is due to the fact that in glassy state the low mobility of nanoparticles hinders the chain orientation caused by slipping on the particle surface.[40] When introducing the nanoparticles, the entropy loss decreases during uniaxial tension, leading to trivial reinforcement. Such a phenomenon was also found in the experimental measurements of nanoparticle/polymer materials.[68] Our simulations can not only reproduce the general features of mechanical properties of nanoparticle-tethering polymers, but also allow us to get a deep insight into the influencing mechanisms of interaction strength and architecture parameters on the mechanical properties, which may provide useful supports for future experiments and material designs.

Nanoparticle-tethering polymer macromolecules are hybrid molecules containing both organic and inorganic components. By using a nanosphere-tethering homopolymer model, the reinforcement mechanisms of nanoparticle-tethering polymers over neat polymers and nanoparticle/polymer blends were elucidated. Importantly, the mechanical reinforcements can be achieved in certain parameter range, such as at strong nanoparticle–polymer nonbonding interactions. The architecture parameters of nanoparticle-tethering polymer molecules, *e.g.*, polymer length and particle size, play important roles in determining the mechanical properties of tethering polymers. The mechanical properties are more diversiform and controllable. The present results demonstrate that connecting polymer tethers to inorganic nanoparticles by covalent bonds provides a promising strategy to create organic/inorganic hybrid materials. According to our studies, through tuning the interaction strength and designing the molecular architecture, hybrid materials with enhanced mechanical properties can be obtained. This is of practical significance for applications in automotive, architectonics, and biomedicine.[7]

4. Conclusions

In the present work, the MD simulations were employed to study the mechanical properties of nanoparticle-tethering polymer systems. The tethering polymers exhibit enhanced mechanical properties relative to neat polymers and nanoparticle/polymer blends. The effects of interaction strength and architecture parameters on the stress–strain behavior of nanoparticle-tethering polymers were examined. The stress was found to increase as the nanoparticle–polymer interaction ε_{np} increases. With decreasing polymer length L or increasing particle size d, the stress increases continuously at smaller strain, while at larger strain the stress first increases and then decreases. In addition, the nanoparticle-tethering polymers possess higher tensional moduli for larger ε_{np}, d or smaller L. The effects of these parameters on mechanical properties were found to be associated with the bond orientation, effective bond length, and nonbonding potential. Our simulation results are in qualitative accordance with available experimental observations. The simulations revealed the principles of diverse mechanical properties of nanoparticle-tethering polymers and may provide useful information for designing and preparing high-performance materials.

Acknowledgements

This work was supported by National Natural Science Foundation of China (21234002, 21304035), Key Grant Project of Ministry of Education (313020) and National Basic Research Program of China (no. 2012CB933600). Support from project of Shanghai municipality (13JC1402000) is also appreciated.

References

1 Q. H. Zeng, A. B. Yu and G. Q. Lu, *Prog. Polym. Sci.*, 2008, **33**, 191–269.
2 G. Choudalakis and A. D. Gotsis, *Eur. Polym. J.*, 2009, **45**, 967–984.
3 L. Zhang and J. Lin, *Macromolecules*, 2009, **42**, 1410–1414.
4 P. Akcora, S. K. Kumar, V. G. Sakai, Y. Li, B. C. Benicewicz and L. S. Schadler, *Macromolecules*, 2010, **43**, 8275–8281.
5 K. Yang and M. Gu, *Polym. Eng. Sci.*, 2009, **49**, 2158–2167.
6 H. J. Taunton, C. Toprakcioglu, L. J. Fetters and J. Klein, *Nature*, 1988, **332**, 712–714.
7 C. Sanchez, P. Belleville, M. Popall and L. Nicole, *Chem. Soc. Rev.*, 2011, **40**, 696–753.

8 X. Zhu, L. Wang, J. Lin and L. Zhang, *ACS Nano*, 2010, **4**, 4979–4988.
9 A. S. Aricò, P. Bruce, B. Scrosati, J. M. Tarascon and W. van Schalkwijk, *Nat. Mater.*, 2005, **4**, 366–377.
10 V. Goel, J. Pietrasik, H. Dong, J. Sharma, K. Matyjaszewski and R. Krishnamoorti, *Macromolecules*, 2011, **44**, 8129–8135.
11 M. K. Corbierre, N. S. Cameron, M. Sutton, K. Laaziri and R. B. Lennox, *Langmuir*, 2005, **21**, 6063–6072.
12 G. G. Vogiatzis and D. N. Theodorou, *Macromolecules*, 2013, **46**, 4670–4683.
13 T. Song, S. Dai, K. C. Tam, S. Y. Lee and S. H. Goh, *Langmuir*, 2003, **19**, 4798–4803.
14 Q. Lan, L. F. Francis and F. S. Bates, *J. Polym. Sci., Part B: Polym. Phys.*, 2007, **45**, 2284–2299.
15 R. Joseph, S. Zhang and W. T. Ford, *Macromolecules*, 1996, **29**, 1305–1312.
16 T. Kawauchi, J. Kumaki and E. Yashima, *J. Am. Chem. Soc.*, 2005, **127**, 9950–9951.
17 Y. Abe, Y. Honda and T. Gunji, *Appl. Organomet. Chem.*, 1998, **12**, 749–753.
18 S. Srivastava, P. Agarwal and L. A. Archer, *Langmuir*, 2012, **28**, 6276–6281.
19 G. Lindenblatt, W. Schärtl, T. Pakula and M. Schmidt, *Macromolecules*, 2001, **34**, 1730–1736.
20 X. H. Wang, S. H. Goh, Z. H. Lu, S. Y. Lee and C. Wu, *Macromolecules*, 1999, **32**, 2786–2788.
21 Y. Han, Y. Xiao, Z. Zhang, B. Liu, P. Zheng, S. He and W. Wang, *Macromolecules*, 2009, **42**, 6543–6548.
22 Y. Wang, X. Wang, X. Zhang, N. Xia, B. Liu, J. Yang, W. Yu, M. Hu, M. Yang and W. Wang, *Chem.–Eur. J.*, 2010, **16**, 12545–12548.
23 N. Miyata, K. Fuke, Q. Chen, M. Kawashita, T. Kokubo and T. Nakamura, *Biomaterials*, 2002, **23**, 3033–3040.
24 A. K. W. Lippach, R. Krämer, M. R. Hansen, S. Roos, K. Stöwe, M. Stommel, G. Wenz and W. F. Maier, *ChemSusChem*, 2012, **5**, 1778–1786.
25 F. Al-Sagheer, A. A. M. Ali, S. Muslim and Z. Ahmad, *Sci. Technol. Adv. Mater.*, 2006, **7**, 111–118.
26 M. Ochi, R. Takahashi and A. Terauchi, *Polymer*, 2001, **42**, 5151–5158.
27 Q. Chen, N. Miyata and T. Kokubo, *J. Am. Ceram. Soc.*, 2003, **86**, 806–810.
28 H. Mahfuz, M. Hasan, V. Dhanak, G. Beamson, J. Stewart, V. Rangari, X. Wei, V. Khabashesku and S. Jeelani, *Nanotechnology*, 2008, **19**, 445702.
29 P. G. Ferreira, A. Ajdari and L. Leibler, *Macromolecules*, 1998, **31**, 3994–4003.
30 A. Jayaraman and K. S. Schweizer, *Macromolecules*, 2008, **41**, 9430–9438.
31 G. D. Smith and D. Bedrov, *Langmuir*, 2009, **25**, 11239–11243.
32 J. Shen, J. Liu, Y. Gao, D. Cao and L. Zhang, *Langmuir*, 2011, **27**, 15213–15222.
33 A. Adnan, C. T. Sun and H. Mahfuz, *Compos. Sci. Technol.*, 2007, **67**, 348–356.
34 J. Cho and C. T. Sun, *Comput. Mater. Sci.*, 2007, **41**, 54–62.
35 O. Borodin, D. Bedrov, G. D. Smith, J. Nairn and S. Bardenhagen, *J. Polym. Sci., Part B: Polym. Phys.*, 2005, **43**, 1005–1013.
36 S. T. Knauert, J. F. Douglas and F. W. Starr, *J. Polym. Sci., Part B: Polym. Phys.*, 2007, **45**, 1882–1897.
37 A. Kutvonen, G. Rossi, S. R. Puisto, N. K. J. Rostedt and T. Ala-Nissila, *J. Chem. Phys.*, 2012, **137**, 214901.
38 S. Fu, X. Feng, B. Lauke and Y.-W. Mai, *Composites, Part B*, 2008, **39**, 933–961.
39 P. R. Mantena, A. Al-Ostaz and A. H. D. Cheng, *Compos. Sci. Technol.*, 2009, **69**, 772–779.
40 J. Liu, S. Wu, L. Zhang, W. Wang and D. Cao, *Phys. Chem. Chem. Phys.*, 2011, **13**, 518–529.
41 R. E. Rudd and J. Q. Broughton, *Phys. Rev. B: Condens. Matter Mater. Phys.*, 1998, **58**, 5893–5896.
42 L. M. Dupuy, E. B. Tadmor, R. E. Miller and R. Phillips, *Phys. Rev. Lett.*, 2005, **95**, 060202.
43 Q. Wang, D. J. Keffer, D. M. Nicholson and J. B. Thomas, *Macromolecules*, 2010, **43**, 10722–10734.
44 S. Sen, S. K. Kumar and P. Keblinski, *Macromolecules*, 2005, **38**, 650–653.
45 Z. Zhang, M. A. Horsch, M. H. Lamm and S. C. Glotzer, *Nano Lett.*, 2003, **3**, 1341–1346.
46 J. Liu, D. Cao and L. Zhang, *J. Phys. Chem. C*, 2008, **112**, 6653–6661.
47 S. Lin, N. Numasawa, T. Nose and J. Lin, *Macromolecules*, 2007, **40**, 1684–1692.
48 J. Liu, Y. Wu, J. Shen, Y. Gao, L. Zhang and D. Cao, *Phys. Chem. Chem. Phys.*, 2011, **13**, 13058–13069.
49 C.-C. Hsieh, S. Jain and R. G. Larson, *J. Chem. Phys.*, 2006, **124**, 044911.
50 K. Kremer and G. S. Grest, *J. Chem. Phys.*, 1990, **92**, 5057–5086.
51 G. S. Grest, K. Kremer and T. A. Witten, *Macromolecules*, 1987, **20**, 1376–1383.
52 J. Liu, Y. Gao, D. Cao, L. Zhang and Z. Guo, *Langmuir*, 2011, **27**, 7926–7933.
53 J. S. Smith, D. Bedrov and G. D. Smith, *Compos. Sci. Technol.*, 2003, **63**, 1599–1605.
54 M. P. Allen and D. J. Tildesley, *Computer Simulation of Liquids*, Clarendon Press, Oxford, 1987.
55 T. Jiang, L. Wang, S. Lin, J. Lin and Y. Li, *Langmuir*, 2011, **27**, 6440–6448.
56 J. E. Mark, *Polymer Data Handbook*, Oxford University Press, Oxford, 2009.
57 J. Gao and J. H. Weiner, *J. Chem. Phys.*, 1995, **103**, 1614–1620.
58 D. R. Rottach, J. G. Curro, G. S. Grest and A. P. Thompson, *Macromolecules*, 2004, **37**, 5468–5473.
59 T. Jiang, L. Wang and J. Lin, *Langmuir*, 2013, **29**, 12298–12306.
60 S. Plimpton, *J. Comput. Phys.*, 1995, **117**, 1–19.
61 C. R. Iacovella and S. C. Glotzer, *Nano Lett.*, 2009, **9**, 1206–1211.
62 A. S. Keys, C. R. Iacovella and S. C. Glotzer, *J. Comput. Phys.*, 2011, **230**, 6438–6463.
63 S. S. Jawalkar, K. V. S. N. Raju, S. B. Halligudi, M. Sairam and T. M. Aminabhavi, *J. Phys. Chem. B*, 2007, **111**, 2431–2439.

64 J. Liu, S. Wu, D. Cao and L. Zhang, *J. Chem. Phys.*, 2008, **129**, 154905.
65 G. Raos and G. Allegra, *J. Chem. Phys.*, 2000, **113**, 7554–7563.
66 L. Zhang, J. Lin and S. Lin, *Soft Matter*, 2009, **5**, 173–181.
67 X. Zhu, L. Wang and J. Lin, *Macromolecules*, 2011, **44**, 8314–8323.
68 D. W. Schaefer and R. S. Justice, *Macromolecules*, 2007, **40**, 8501–8517.